Journal of Alloys and Compounds 303–304 (2000) 182–190
Journal of ALLOYS AND COMPOUNDS
www.elsevier.com/locate/jallcom

Spectroscopic characterization of trivalent f-element (Eu, Am) solid carbonates

W. Runde[a,]*, C. Van Pelt[a], P.G. Allen[b]

[a]Los Alamos National Laboratory, Chemical Science and Technology Division, MS J514, Los Alamos, NM 87545, USA
[b]Lawrence Livermore National Laboratory, Seaborg Institute for Transactinium Science, Livermore, CA 94551, USA

Received 15 July 1999

Abstract

Solubility studies show that trivalent f-element carbonate compounds are the predominant solids that primarily limit the soluble metal ion concentration under environmental conditions. We systematically investigated the spectroscopic characteristics of a series of solid f-element (Eu and ^{243}Am) carbonates. Varying pH, ionic strength, and carbonate concentration results in the formation of $M(OH)_3$, $MOHCO_3$, $M_2(CO_3)_3 \cdot nH_2O$, and $NaM(CO_3)_2 \cdot nH_2O$, where M=Eu(III) or Am(III). Solids were characterized by FTIR, fluorescence, and EXAFS spectroscopies that determined and confirmed the coordination environment, and by their individual X-ray diffraction powder patterns. The number of coordinated crystal waters was determined to be 2–3 for $Eu_2(CO_3)_3 \cdot nH_2O$ and 5 for $NaEu(CO_3)_2 \cdot nH_2O$ using thermogravimetric/differential thermal analysis and fluorescence lifetime. We report studies of the fluorescence of Am(III) and the effect of carbonate coordination on the $^5D_1 \rightarrow {}^7F_1$ transition.

Keywords: Europium; Carbonate; Fluorescence; EXAFS

1. Introduction

Solid M(III) carbonates have been determined to be the predominant solubility-controlling phases for trivalent f-elements under conditions relevant to natural environments [1]. In the absence of carbonate, $M(OH)_3$ precipitates under normal conditions, while $MOHCO_3$ [1,2], $M_2(CO_3)_3 \cdot nH_2O$ [1–3], and $NaM(CO_3)_2 \cdot nH_2O$ [4], where M=Ln(III) or An(III), form with varying CO_2 partial pressure, pH, and ionic strength. The study of solid–liquid phase equilibria requires knowledge on the nature of the solid phases involved in order to interpret and predict solution speciation accurately [5,6]. Since most solid Ln(III) and An(III) carbonate phases appear to be amorphous and thus cannot be characterized by using X-ray powder diffraction [7,8], limited structural information are available for these compounds.

Crystalline phases of the orthorhombic ancylite-type structure $MOHCO_3$ have been reported for La–Eu [9] and two crystal structures for $NdOHCO_3$ have been proposed based on optical determination of ligand site symmetries and X-ray diffraction powder pattern [10]. While the single crystal structure of $La_2(CO_3)_3 \cdot 8H_2O$ has been reported [11], no definitive crystal structures are known for the tengerite-type $Ln_2(CO_3)_3 \cdot 2\text{–}3H_2O$ [12–14]. Beside IR spectra and X-ray diffraction powder patterns no structural data are available for the double carbonates [15,16]. Information on coordination and bond lengths can be obtained from the recently reported crystal structure of $Na_3Eu(CO_3)_3$ which was synthesized hydrothermally at 220 °C [17].

Spectroscopic techniques, such as FTIR, time-resolved laser fluorescence or X-ray absorption spectroscopies, have been used to obtain structural information of less crystalline and amorphous compounds. The fluorescence properties of Eu(III) salts (i.e. chloride [18,19], fluoride [20,21]) or of Eu(III) doped in host matrices (i.e. $LaCl_3$ [22] or YVO_4 [23]) have been investigated extensively providing information on the coordination environment of Ln(III) ions and electrostatic crystal field models. Eu(III) fluorescence has been applied for speciation in solution and solid states [24–31], but only Eu(III) carbonato complexes in solution have been characterized. The fluorescence of Am(III) has not been studied near the extent of Eu(III) or Cm(III) probably due to its relatively short fluorescent lifetime (nanosecond range). However, Am(III) fluorescence has been applied for trace determination with

*Corresponding author. Fax: +1-505-665-4955.

0925-8388/00/$ – see front matter
PII: S0925-8388(00)00665-4

a detection limit of 10^{-10} M in a solid host matrix of ThO_2 [32].

The present work focuses on the spectroscopic characterization of M(III) solid carbonates, with M=Eu and Am, most relevant for aqueous solid–liquid phase equilibria [2,4,5,7,17,28,33–38]. The choice of the two elements is based on their similar f-electron configurations, ionic radii, and complexation properties. X-ray powder diffraction is used to identify the solids, and Extended X-Ray Absorption Fine Structure (EXAFS) and fluorescence spectroscopy are employed to study the structural properties and to determine the hydration number.

2. Experimental details

The preparation of the M(III) carbonate compounds followed well-known literature procedures by applying different CO_2 partial pressures (air, argon with 1% CO_2, and pure CO_2 gas). $MOHCO_3$ was synthesized in 0.1 M $NaClO_4$ under 0.03% CO_2 partial pressure [2]; $M_2(CO_3)_3\cdot nH_2O$ was precipitated in 0.001 M Na_2CO_3 solution under 100% CO_2 atmosphere in 0.1 M $NaClO_4$ [2]; the M(III) sodium carbonate, $NaM(CO_3)_2\cdot nH_2O$, was obtained in alkaline 5 M NaCl solution under 100% CO_2. The solid phases were analyzed using X-ray diffraction (INEL, XPS-400), thermogravimetric (TG) and differential thermoanalysis (DTA) (Thermo Jarrell Ash, ThermoSpec/AE), FTIR (Nicolet, Magna IR560), time resolved laser fluorescence spectroscopy (TRLFS), and EXAFS.

The TRLFS experiments were performed using a Nd-YAG pulsed laser (Spectra-Physics GCR-100 series) coupled to an optical parametric oscillator (Quanta Ray MOPO-700) with a pulse frequency of 10 Hz and a pulse width of 5 ns. The fluorescence was detected using a photomultiplier tube after passing through the emission monochromator (Photon Technology, Inc.). Eu(III) excitation at 396 nm was used while the fluorescence was monitored between 570 and 710 nm. Am(III) excitation was set at 504 nm and emission was monitored between 660 and 740 nm. Lifetimes were collected by monitoring emission at 614 nm for Eu(III) and at 691 nm for Am(III) at 691 nm.

2.1. XAS data acquisition and analysis

Europium L_{III}-edge X-ray absorption spectra were collected at the Stanford Synchrotron Radiation Laboratory (SSRL) on bending magnet beamline 2–3 (unfocused) under dedicated ring conditions (3.0 GeV, 50–100 mA). Samples mixed with BN powder were individually loaded into an Oxford Instruments continuous-flow liquid helium cryostat, and the XAS experiments were performed at 20 K. A Si (220) double-crystal monochromator was employed using a vertical slit of 1.0 mm to maintain adequate flux while achieving good resolution. Rejection of higher order harmonic content of the beam was achieved by detuning θ, the angle between crystals in the monochromator, such that the incident flux was reduced to 50% of its maximum (>95% harmonic is rejected). All spectra were collected in the transmission geometry using nitrogen-filled ionization chambers. The spectra were energy calibrated by simultaneously measuring the spectrum from the reference compound, Eu_2O_3. The first inflection point of the absorption edge for the reference was defined as 6977 eV. EXAFS data were extracted from the raw absorption spectra by standard methods described elsewhere [39] using the suite of programs EXAFSPAK developed by G. George of SSRL. Non-linear least squares curve-fitting analysis was done using EXAFSPAK to fit the raw k^3-weighted EXAFS data. The theoretical EXAFS modeling code, FEFF7, of Rehr et al. [40] was employed to calculate the backscattering phases and amplitudes of the individual neighboring atoms for curve-fitting the raw data. The amplitude reduction factor, S_o^2, was held fixed at 0.8 for all of the fits. The shift in threshold energy, ΔE_0, was allowed to vary as a global parameter for all shells in each of the fits.

3. Results and discussion

3.1. Stability and characterization

Trivalent lanthanide and actinide carbonates precipitate with dependence on carbonate concentration, pH, and ionic strength. The M(III) hydroxocarbonate, $MOHCO_3$, is stable only under conditions where hydrolysis and carbonate complexation are concurrent reactions, namely at both low pH and CO_2 partial pressures. At elevated CO_2 partial pressures ($\geq 10^{-2}$ atm) the M(III) normal carbonate, $M_2(CO_3)_3\cdot nH_2O$, precipitates. The transition reaction 2 $M(OH)CO_3(s)+CO_3^{2-}\rightarrow M_2(CO_3)_3(s)+2OH^-$ is driven by the pH and the CO_2 partial pressure which govern the ratio $[OH^-]/[CO_3^{2-}]$ in solution. Under conditions of equal stability of $MOHCO_3$ and $M_2(CO_3)_3\cdot nH_2O$, the formation of the first complexation products, MOH^{2+} and MCO_3^+ should be balanced:

$$[MOH^{2+}]/[MCO_3^+] = (\beta'_{110}/\beta'_{101})\cdot([OH^-]/[CO_3^{2-}]) = 1 \quad (1)$$

where β'_{110} and β'_{101} are the apparent formation constants of MOH^{2+} and MCO_3^+. Using the reported stability constants for Eu(III), log $\beta'_{110}=5.42$ [41] and log $\beta'_{101}=5.8$ [41] the hydroxide concentration is approximately double the carbonate concentration. With decreasing concentration ratios, the formation of the normal carbonate is favored and, at higher ionic strength, the formation of the alkali carbonate, $NaM(CO_3)_2\cdot nH_2O$, is preferred.

The X-ray powder diffraction patterns of the Eu(III) solid phases are shown in Fig. 1. The XRD data for

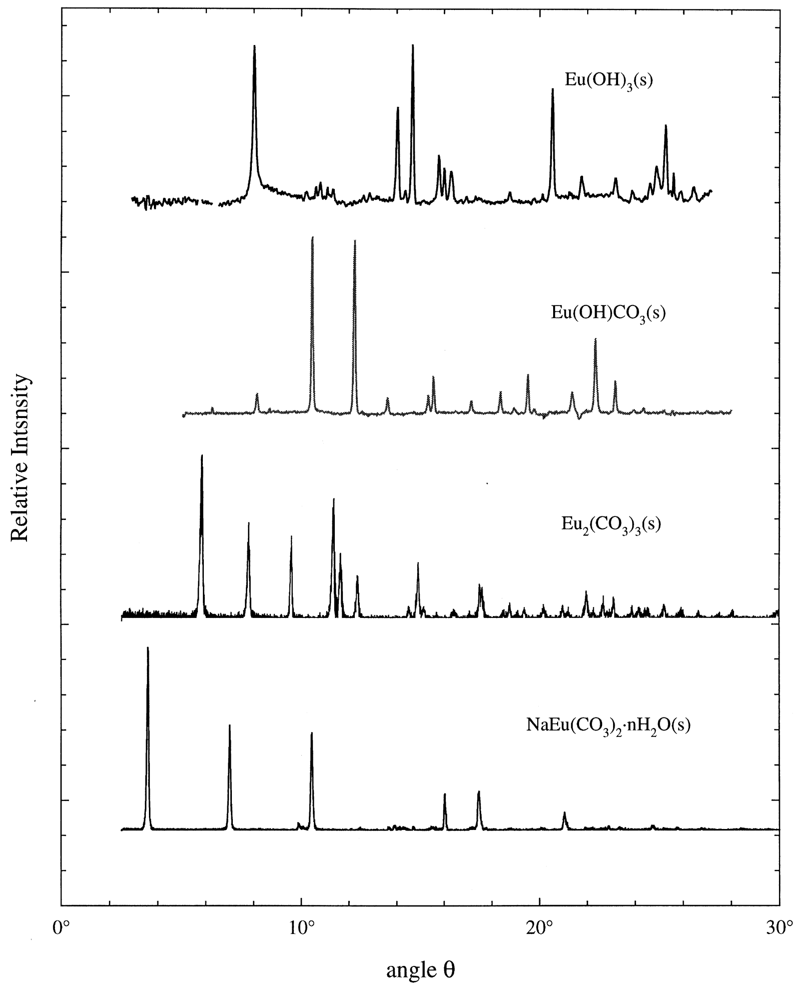

Fig. 1. X-ray diffraction powder pattern of $Eu(OH)_3$, $Eu(OH)CO_3$, $Eu_2(CO_3)_3 \cdot nH_2O$, and $NaEu(CO_3)_2 \cdot nH_2O$.

$MOHCO_3$ (M = Nd, Eu, Am) [2] and $M_2(CO_3)_3 \cdot 2–3\ H_2O$ (M = Nd, Eu) [2,3] were discussed previously and the data for $NaM(CO_3)_2 \cdot 5H_2O$ (M = Nd, Eu, Am) are given in Table 1. The powder diffraction patterns compare well with each other and with those given in the literature. No Bragg reflections were observed for the Am(III) normal carbonates and only weak peaks for the double carbonate indicating the amorphous character of these solids. We interpreted the Bragg reflections of $NaM(CO_3)_2 \cdot 5H_2O$ with a tetragonal cell with $a = 1303(3)$ pm for Nd(III) (1311 pm [42]), 1300(2) for Eu(III), and 1307(4) pm for Am(III), and $c = 994(3)$ pm for Nd(III) (993 pm [42]), 995(2) pm for Eu(III), and 993(6)) pm for Am(III). This is in agreement with the reported tetragonal symmetry of $NaM(CO_3)_3 \cdot 5H_2O$ (M = Nd, Sm, Gd, Dy) with eight molecules per unit cell [42]. The peak at low 2θ values is indicative of the presence of intercalated alkali cations and the increased distance between the Eu(III) carbonate layers and can be used for fast identification of the double carbonate. Further structural information, such as coordination number or bond lengths, cannot be obtained from the Bragg reflections and additional spectroscopic techniques have to be applied.

We used FTIR and DTA/TGA to investigate the coordination of hydration water. $MOHCO_3$ (M = Nd, Eu) does not contain any waters of hydration [2,3]. The hydroscopic character of the normal carbonates complicates the accurate determination of the numbers of coordinated water molecules and between two and three coordinated water molecules are observed for $Eu_2(CO_3)_3 \cdot 2–3\ H_2O$ [2,3]. The thermogravimetric decomposition for the alkali carbonate, $NaEu(CO_3)_2 \cdot 5H_2O$, shows the dehydration of five coordinated water molecules in the range 65°–105°C. The presence of water molecules, either coordinated or adsorbed, in $Eu_2(CO_3)_3 \cdot 2–3H_2O$ and $NaEu(CO_3)_2 \cdot 5H_2O$ is reflected by their broad FTIR bands at about 3400 cm^{-1}. The FTIR spectrum of $EuOHCO_3$ exhibits a very narrow band at 3479 cm^{-1} confirming a coordinated hydroxo group and the absence of water molecules. These observations agree well with those reported for $Nd_2(CO_3)_3 \cdot nH_2O$ and $NdOHCO_3$ [2]. The symmetric and asymmetric stretching frequencies of $NaEu(CO_3)_2 \cdot 5H_2O$ at 1686 and

Table 1
Bragg reflections of $NaM(CO_3)_2 \cdot nH_2O$ (M = Nd, Eu, Am) in comparison with literature data (in parentheses) for Am(III) [7] and Nd(III) [42]. X-ray powder diffraction patterns of $M(OH)CO_3$ and $M_2(CO_3)_3 \cdot nH_2O$ are discussed in [2][a]

Indices hkl	$NaNd(CO_3)_2(s)$		$NaEu(CO_3)_2(s)$		$NaAm(CO_3)_2(s)$	
	Rel. int. in %	d in pm	Rel. int. in %	d in pm	Rel. int. in %	d in pm
100	70	1307 (1298)	60	1301	100	1310 (1303)
200	40	653 (649)	30	649	50	654 (650)
102	100	464 (464)	100	457	60	458 (462)
300	90	435 (433)	70	431	60	434 (433)
221	30	414 (417)				(416)
202	30	394 (394)				(394)
		(325)	60	330	30	329
400	40	324 (325)	60	321	70	325
103	50	319 (321)	50	319	40	319 (320)
140	50	315 (315)	40	316		
113	20	313 (311)				(313)
			80	307	40	309 (310)
	10	301	10	301	10	299
203	30	295 (295)	20	295		
240	20	291 (290)	20	292	20	293 (295)
213	10	288 (288)	30	286	20	287 (287)
223, 142	20	268 (269)				
303	20	261 (263)				
133	40	258 (258)	<10	257	30	259 (259)
521	10	234 (234)				(257)
403, 502	10	231 (232)				(232)
124	20	229 (230)	<10	228	10	227 (228)
	40	225 (228)	10	225	10	224
531	30	217 (217)	20	216	10	215
	20	209	30	208	<10	209
	20	207	30	205		
	20	203	<10	202		
	10	200	10	201	<10	200 (196)

Lattice constants:	$NaNd(CO_3)_2(s)$	$NaEu(CO_3)_2(s)$	$NaAm(CO_3)_2(s)$
[a] a_o:	1303±3 pm (1311 pm [15])	1300±2 pm	1307±4 pm
c_o:	994±3 pm (993 pm [15])	995±1 pm	993±6 pm

1518 cm^{-1}, respectively, differ significantly from those of the other Eu(III) carbonates ($EuOHCO_3$: 1510 and 1433 cm^{-1}; $Eu_2(CO_3)_3 \cdot 2–3H_2O$: 1499 and 1406 cm^{-1}) and can be used for solid phase identification.

3.2. EXAFS

We applied EXAFS spectroscopy to determine bond lengths and coordination numbers in the Eu(III) solids. The raw k3-weighted EXAFS data and the corresponding Fourier Transforms (FT) for the Eu(III) compounds are shown in Fig. 2. The FT represents a pseudo-radial distribution function and the peaks are shifted to lower *R* values as a result of the phase shifts associated with the absorber–scatterer interactions (~0.2–0.5 Å). The FT moduli show peaks associated with Eu–O, Eu–C, and Eu–Eu interactions in these compounds. In all of the samples, the FT peak at 2.0 Å is due to backscattering from the first shell O neighbors which originate from either the hydroxo or carbonate ligands (bidentate and monodentate bond geometries). The FT peaks located at ca. 4.0 Å in the spectra of $Eu(OH)_3$ and $EuOHCO_3$ are principally due to Eu–Eu interactions. The complex series of smaller peaks in the vicinity of 3–4 Å for $Eu_2(CO_3)_3 \cdot nH_2O$ and $NaEu(CO_3)_2 \cdot nH_2O$ are due to scattering paths from the C and O atoms in mono- and bidentate bonded carbonate groups as well as Eu–Eu interactions.

The results of non-linear least squares curve-fitting to the k^3-weighted EXAFS data are shown in Table 2. A preliminary set of fits was performed on the $Eu(OH)_3$, $EuOHCO_3$, and $Eu_2(CO_3)_3 \cdot nH_2O$ compounds to determine the extent of agreement between these EXAFS results and previously published XRD structures. EXAFS interactions in the $Eu(OH)_3$, $EuOHCO_3$, and $Eu_2(CO_3)_3 \cdot nH_2O$ solids were found to be consistent with the respective hexagonal, orthorhombic ancylite-type, and orthorhombic tengerite-type structures of these compounds. The EXAFS results were not consistent with the hexagonal form of $EuOHCO_3$ or the lanthanite structure in $Eu_2(CO_3)_3 \cdot nH_2O$. As a result, the final curve-fits were

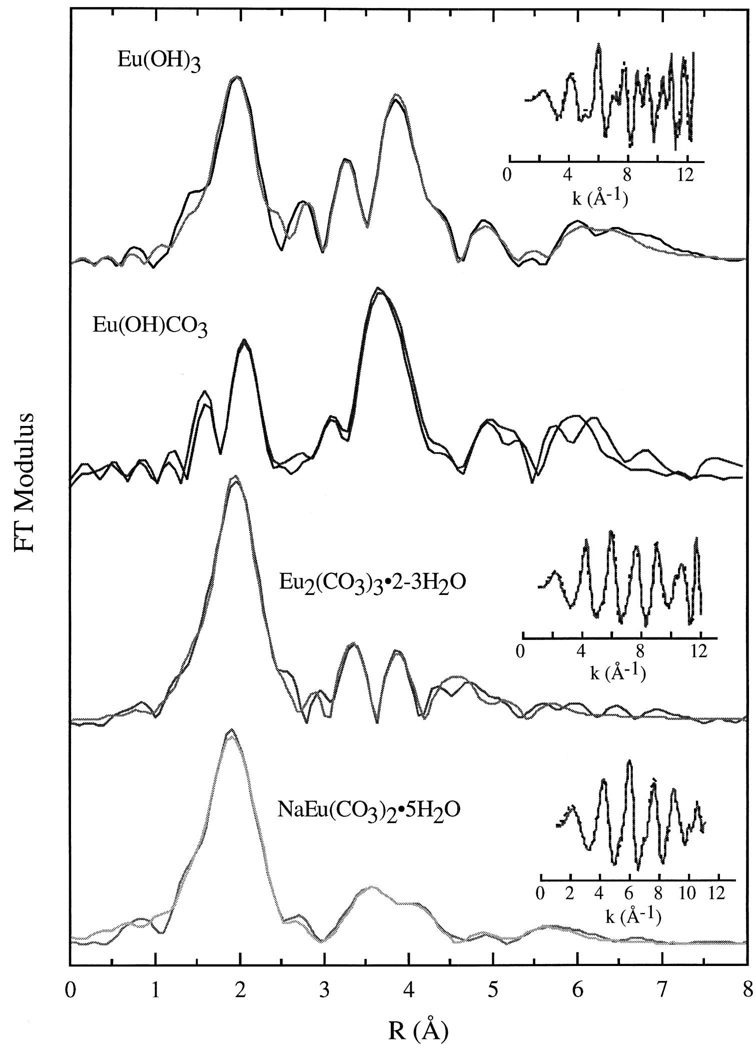

Fig. 2. EXAFS data of $Eu(OH)_3$, $Eu(OH)CO_3$, $Eu_2(CO_3)_3 \cdot nH_2O$, and $NaEu(CO_3)_2 \cdot nH_2O$.

Table 2
Bond distances and coordination numbers in Eu(III) carbonate solids determined by EXAFS

Sample	Shell	*R* (Å)[a]	*N*	σ^2 (Å^2)	*R* (average from XRD model)
$Eu(OH)_3$	Eu–O	2.46	9	0.0053	2.47
	Eu–Eu	3.66	2	0.0029	3.65
	Eu–O	3.93	3	0.0045	3.92
	Eu–Eu	4.11	6	0.0029	4.10
$EuOHCO_3$	Eu–O	2.51	9	0.0110	2.58
	Eu–Eu	3.82	2	0.0010	3.90
	Eu–Eu	4.20	2	0.0010	4.27
$Eu_2(CO_3)_3 \cdot 2–3H_2O$	Eu–O	2.45	9	0.0051	2.46
	$Eu–C_{bi}$	2.88	3	0.0051	2.86
	$Eu–O_{distal}$	4.17	3	0.0034	4.15
	Eu–Eu	4.17	2	0.0008	4.16
$NaEu(CO_3)_2 \cdot 5H_2O$	Eu–O	2.46	9	0.0076	–
	$Eu–C_{bi}$	2.89	3	0.0053	–
	$Eu–C_{mono}$	3.57	3	0.0066	–
	$Eu–O_{distal}$	4.22	3	0.0034	–

[a] The standard deviations (1σ) for *R* as estimated by EXAFSPAK are: Eu–O, $R \pm 0.003$ Å; Eu–C, $R \pm 0.005$ Å; and Eu–Eu, $R \pm 0.008$ Å.

done by fixing the coordination numbers, *N*, at their average crystallographic values and by varying the bond lengths, *R*, and the Debye–Waller factors, σ, for the various shells. The bond lengths obtained from EXAFS are in good agreement with the average crystallographic *R*-values (also shown in Table 2). It should be noted that the Eu–OCO_2 bond lengths also agree with the Ce–O bond lengths reported for $Ce(CO_3)_5^{6-}$ (2.379 – 2.504 Å) [43,44]. Although XRD data has been obtained for the double carbonate solid $NaEu(CO_3)_2 \cdot nH_2O$, specific details (*R* and *N* values) of the structure have not been reported. Initial inspection of both the EXAFS k-space and FT plots suggests that the Eu coordination in $NaEu(CO_3)_2 \cdot nH_2O$ resembles the Eu coordination in $Eu_2(CO_3)_3 \cdot nH_2O$. As a result, the EXAFS spectrum for $NaEu(CO_3)_2 \cdot nH_2O$ was modeled based on structural details from the $Eu_2(CO_3)_3 \cdot nH_2O$ structure. EXAFS results for the double carbonate reveal monodentate and bidentate carbonate coordination. Monodentate coordination is known to be present in the $Eu_2(CO_3)_3 \cdot nH_2O$ structure, however, it was not detected in the EXAFS data probably as a result of static disorder present in this compound. The coordination environment in the Eu(III) carbonate solids are also in good agreement with the structure of the recently reported $Na_3Eu(CO_3)_3$ [17] in which the Eu atom is coordinated to nine oxygen atoms from six carbonate ligands (three carbonates are bidentate via two oxygen atoms while the three remaining ligands are monodentate).

3.3. Fluorescence

The emission spectra of Eu(III) solution complexes exhibit broad peaks for the main transitions $^5D_0 \rightarrow {}^7F_J$ ($J=1,2$) [28]. In contrast, well-resolved bands are observed for the transitions in the Eu(III) solid carbonates (Fig. 3). The emission spectra ($\lambda_{exc}=394.3$ nm) of the Eu(III) solids are dominated by the electronic transitions from the $^5D_0$ level to the ^7F_J ($J=0$–4) multiplet. In contrast to the fluorescence of Eu(III) solution species, additional transitions in the solid state of Eu(III) from the $^5D_1$ level can be observed. Characteristic shifts in the peak maxima and intensities of the hypersensitive band $^5D_0 \rightarrow {}^7F_2$ change significantly with coordination [45]. The latter transition shows the highest intensity among all observable emission peaks as also observed in Eu(III) solution species. Table 3 summarizes the observed peak maxima at room temperature. The peaks at about 575 nm relate to the $^5D_0 \rightarrow {}^7F_0$ transition and their multiplicity defines the number of different coordination environments around the europium [24,25]. Only single peaks are observed in each spectra indicating the presence of single phases with one Eu(III) coordination environment. The emission spectra of $Eu(OH)_3$ show only a few well-resolved transitions and the peaks are broadened due to enhanced O–H vibrations at room temperatures. The peak positions presented here are in reasonable agreement with the data taken at 4.2 K [46]. The higher splitting pattern of the carbonates suggests a lower symmetry than in $Eu(OH)_3$, which crystallizes in a hexagonal form of the UCl_3 type with space group $P6_3/m$ (C_{6h}^2) [46]. The different coordination of Eu(III) with hydroxide and carbonate causes a significant splitting into discrete crystal field levels that allows the distinction of Eu(III) solid carbonates using TRLFS.

In contrast to the resolved Eu(III) fluorescence bands in the solid state, only broad peaks exhibit the emission

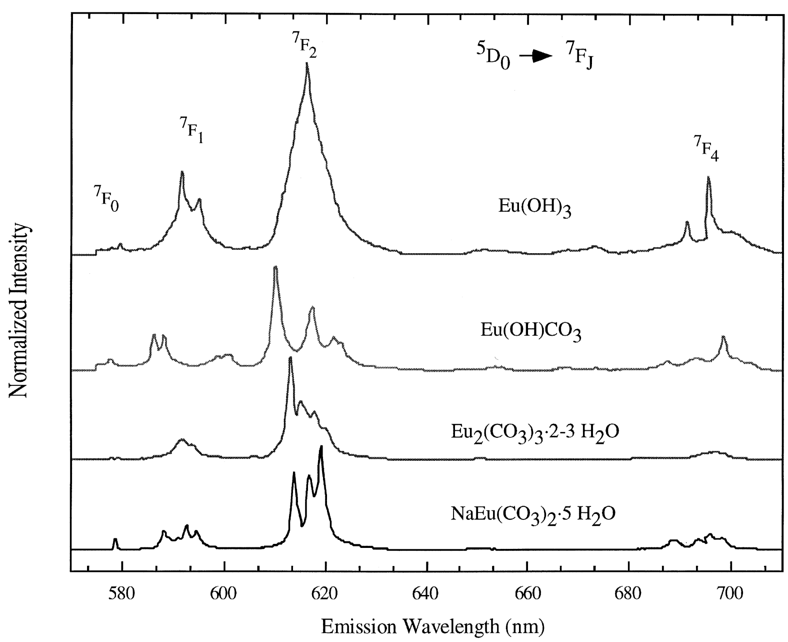

Fig. 3. Fluorescence spectra of $Eu(OH)_3$, $Eu(OH)CO_3$, $Eu_2(CO_3)_3 \cdot nH_2O$, and $NaEu(CO_3)_2 \cdot nH_2O$.

Table 3
Fluorescence peak positions (nm) of Eu(III) and Am(III) carbonate solids. Literature data of $Eu(OH)_3$ at 4.2 K are given for comparison in parenthesis [48]

Transition	$Eu(OH)_3$	$Eu(OH)CO_3$	$Eu_2(CO_3)_3 \cdot nH_2O$	$NaEu(CO_3)_2 \cdot nH_2O$
$^5D_1 \rightarrow ^7F_1$	535.70		536.11	
$^5D_1 \rightarrow ^7F_2$	550.51		552.46	
$^5D_1 \rightarrow ^7F_3$	583.36			
$^5D_0 \rightarrow ^7F_0$	577.50	577.47	579.24	578.80
$^5D_0 \rightarrow ^7F_1$	591.40 (592.1)	586.17	591.40	588.17
	594.88 (595.6)	587.92	593.61	592.52
	(616.8)	600.10	606.21	594.46
$^5D_0 \rightarrow ^7F_2$	616.26	610.13	613.16	613.65
		617.09	615.12	616.71
		621.23	617.51	619.08
$^5D_0 \rightarrow ^7F_3$	652.19 (651.9)	656.64	651.08	649.77
$^5D_1 \rightarrow ^7F_5$	667.60	670.20	672.81	
	673.31			
$^5D_0 \rightarrow ^7F_4$	691.13 (690.6)	687.38	683.71	688.47
	695.70 (696.6)	692.86	696.77	693.53
	698.52 (697.9)	698.52		695.94
	700.28	703.28		698.57
$^5D_1 \rightarrow ^7F_6$	715.51	714.59		
$^5D_0 \rightarrow ^7F_5$	748.22 (747.8)			
	(751.6)			
	761.90 (757.6)	756.37	764.00	745.99
Lifetime (μs)	21.6±3.3	109.8±7.7	233.6±9.8	207.7±8.2
Transition	Am^{3+}	$Am(CO_3)_3^{3-}$	$Am(OH)CO_3$	$NaAm(CO_3)_2 \cdot nH_2O$
$^7F_0 \rightarrow ^5L_6$	503.2	507.7		
$^5D_1 \rightarrow ^7F_1$	686.9	694.6	699.6	702.0
Lifetime (ns)	20.4±2.1	34.5±2.4		

spectra of Am(III) in both solution and solid state (Fig. 4). Excitation of Am(III) to the $^5L_6$ excited state from the $^7F_0$ ground state (504 nm) results in the emission from the lowest luminescent level to the ground state manifold. The two most populated transitions are the $^5D_1 \rightarrow ^7F_1$ band at 685 nm and $^5D_1 \rightarrow ^7F_2$ band at 836 nm. The fluorescence peak of Am^{3+}(aq) at 685 nm is shifted with carbonate complexation towards higher wavelengths and the fluorescence for the triscarbonato complex, $Am(CO_3)_3^{3-}$, is observed at 693 nm. Thus far, we were unable to obtain fluorescence data on the Am(III) mono- and biscarbonato complex due to the low solubility of Am(III) at lower carbonate concentration.

The fluorescence decay rate is dependent on its inner coordination sphere and radiative and non-radiative processes. The O–H oscillator is known to quench the fluorescent lifetimes and decrease fluorescence intensities due to the coupling of the fluorescent probe's excited states to the vibrational overtones of the coordinated O–H oscillators [25–27]. Consequently, with the replacement of inner-sphere coordinated water molecules against carbonate ligands, the lifetime increases from Am^{3+}(aq) to $Am(CO_3)_3^{3-}$ and follows the reported trend for Eu(III) [28] and Cm(III) [28,47] solution complexes. The correlation between inner-sphere water molecules and lifetime of the excited state can be used to determine the hydration number. We applied the linear relationship developed by Horrocks [26,27] and Choppin [48],

$$n_{H_2O} = x \cdot \tau_{H_2O}^{-1} - y \tag{2}$$

to calculate the number of associated hydration waters for Eu(III) solid carbonates and Am(III) solution species. Choppin [48] determined the values to be $x = 1.05$ and $y = 0.70$ for Eu(III) and Kimura [49] determined $x = 2.56 \times 10^{-7}$ and $y = 1.43$ for Am(III). We applied those data accordingly and obtained the following number of coordinated water molecules:

Species	Lifetime	Inner sphere waters
$Eu_2(CO_3)_3 \cdot 2–3H_2O$	234±10 μs	2.8±0.5
$NaEu(CO_2)_2 \cdot 5H_2O$	208±8 μs	4.5±0.5
Am^{3+}(aq)	20.4±2.1 ns	11.1±0.5
$Am(CO_3)_3^{3-}$	34.5±2.4 ns	6.0±0.5

The resulting numbers of hydration for $Eu_2(CO_3)_3 \cdot 2–3H_2O$, 2.8±0.5, and $NaEu(CO_2)_2 \cdot 5H_2O$, 4.5±0.5, confirm the results from our DTA/TGA measurements. The hydroxo group in $MOHCO_3$ does not allow the determination of the hydration numbers due to the quenching of

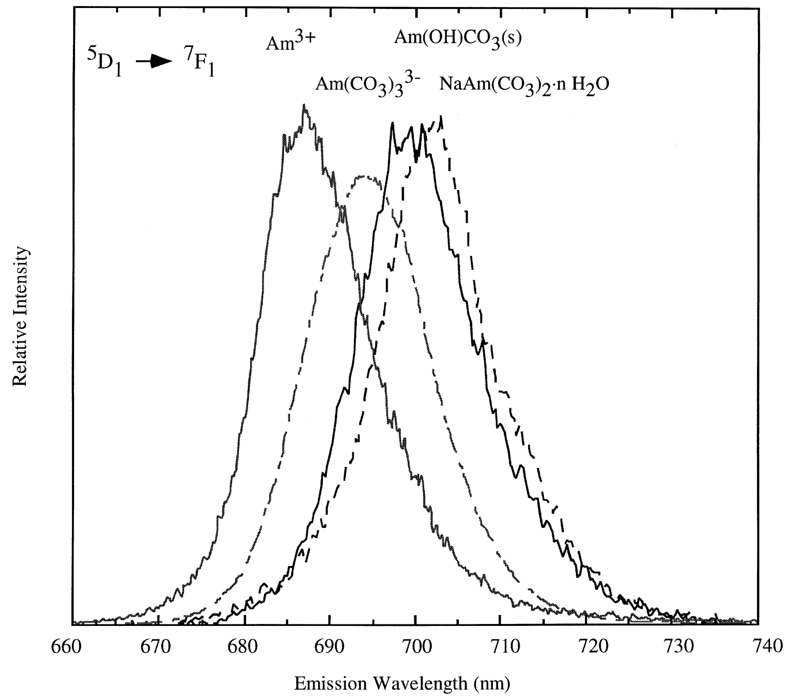

Fig. 4. Fluorescence spectra of Am^{3+}(aq), $Am(CO_3)_3^{3-}$, $Am(OH)CO_3$, and $NaAm(CO_3)_2 \cdot nH_2O$.

the coordinated OH group. The lifetime of the Am^{3+}(aq) emission matches well the reported value of 24.6±0.6 ns [49] and 22.3 ns [50] in aqueous systems while the number of hydration waters derived using Eq. (2) is higher than those previously reported (9 [49]; 10.5 [50]). This deviation may be caused by the short lifetime of the Am(III) species and the limitations of the spectroscopic equipment.

4. Conclusion

Solid phases of trivalent f-elements have been mainly characterized using powder X-ray diffraction patterns. The amorphous nature of most actinide(III) solids relevant for environmental conditions excludes this technique for adequate characterization and identification. Spectroscopic techniques have been used to fully characterize amorphous and crystalline Eu(III) and Am(III) solid carbonates. Fluorescence and EXAFS spectra are unique identifiers and were used to successfully study the coordination environment of Eu(III) and Am(III) carbonates in solution and in solid state.

Acknowledgements

This research was supported by the Laboratory Directed Research and Development Program Actinide CD Thrust at Los Alamos National Laboratory and by Lawrence Livermore National Laboratory under Contract No. W-7405-ENG-48. XAS experiments were performed at the Stanford Synchrotron Radiation Laboratory (SSRL), which is operated by the Department of Energy, Division of Chemical Sciences. Additional support for P.G. Allen was provided by the Actinide Chemistry Group at Lawrence Berkeley National Laboratory which is funded by the Office of Basic Energy Sciences, Department of Energy under Contract No. DE-AC03-76SF00098.

References

[1] P. Vitorge, Radiochim. Acta 58–59 (1992) 105–107.
[2] W. Runde, G. Meinrath, J.I. Kim, Radiochim. Acta 58–59 (1992) 93–100.
[3] G. Meinrath, J.I. Kim, Radiochim. Acta 52–53 (1991) 29–34.
[4] L.F. Rao, D. Rai, A.R. Felmy, R.W. Fulton, C.F. Novak, Radiochim. Acta 75 (1996) 141–147.
[5] J.I. Kim, Mat. Res. Soc. Symp. Proc. 294 (1993) 3–21.
[6] H. Nitsche, Mat. Res. Soc. Symp. Proc. 212 (1991) 517–529.
[7] G. Meinrath, Carbonat-Komplexierung des Dreiwertigen Americiums unter Grundwasserbedingungen; Instituit für Radiochemie, TU München, 1991.
[8] R.J. Silva, G. Bidoglio, M.H. Rand, P.B. Robouch, H. Wanner, I. Puigdomenech, Chemical Thermodynamics of Americium, Vol. 2, North-Holland Elsevier Science Publishers B.V., Amsterdam, 1995.
[9] M. Ankic, D.J. Sordelet, M. Munson, Adv. Cer. Mat. 3 (1988) 211–216.
[10] H. Dexpert, P. Caro, Mat. Res. Bull. 9 (1974) 1577–1586.
[11] D.B. Shinn, H.A. Eick, Inorg. Chem. 7 (1968) 1340–1345.
[12] P.E. Caro, J.O. Sawyer, L.R. Eyring, Spectrochim. Acta 28A (1972) 1167.
[13] K. Nagashima, H. Wakita, A. Mochizuki, Bull. Chem. Soc. Japan 46 (1973) 152–156.
[14] S. Liu, R. Ma, R. Jiang, F.J. Luo, Cryst. Growth 203 (1999) 454–457.

[15] A. Mochizuki, K. Nagashima, H. Wakita, Bull. Chem. Soc. Japan 47 (1974) 755–756.
[16] H. Schweer, H.Z. Seidel, Anorg. Allg. Chem. 477 (1981) 196–204.
[17] N. Mercier, M. Leblanc, E. Antic-Fidancev, M. Lemaitre-Blaise, J. Solid State Chem. 132 (1997) 33–40.
[18] E.V. Sayre, S. Freed, J. Chem. Phys. 24 (1956) 1211–1213.
[19] K.H. Hellwege, Ann. Phys. 40 (1941) 529.
[20] H.H. Caspers, H.E. Rast, J. Chem. Phys. 47 (1967) 4505–4514.
[21] N. Mercier, E. Antic-Fidancev, M. Lemaitre-Blaise, M. Leblanc, J.-C. Krupa, J. Alloys Comp. 275–277 (1998) 416–419.
[22] L.G. DeShazer, G.H. Dieke, J. Chem. Phys. 38 (1963) 2190–2199.
[23] C. Brecher, H. Samelson, A. Lempicki, R. Riley, T. Peters, Phys. Rev. 155 (1967) 178–187.
[24] J.-C.G. Bünzli, in: J.-C.G. Bünzli, G.R. Choppin (Eds.), Luminescent Probes, Elsevier, New York, 1989, pp. 219–293.
[25] G.R. Choppin, D.R. Peterman, Coord. Chem. Rev. 174 (1998) 283–299.
[26] W.D. Horrocks Jr., D.R. Sudnick, Science 206 (1979) 1194–1196.
[27] W.D. Horrocks Jr., D.R. Sudnick, Acc. Chem. Res. 14 (1981) 384–392.
[28] J.I. Kim, R. Klenze, H. Wimmer, W. Runde, W. Hauser, J. Alloys Comp. 213 (1994) 333–340.
[29] W.T. Carnall, in: K.A. Gschneidner Jr., L.R. Eyring (Eds.), The Absorption and Fluorescence Spectra of Rare Earth Ions in Solution, Vol. 3, North-Holland Publishing Company, New York, 1979.
[30] T. Kimura, G.R. Choppin, Y. Kato, Z. Yoshida, Radiochim. Acta 72 (1996) 61–64.
[31] Z. Wang, G.R. Choppin, P. Di Bernardo, P.-L. Zanonato, R. Portanova, M. Tolazzi, J. Chem. Soc., Dalton Trans. (1993) 2791–2796.
[32] P. Thouvenot, S. Hubert, C. Moulin, P. Decambox, P. Mauchien, Radiochim. Acta 61 (1993) 15–21.
[33] J. Fuger, I.L. Khodakovsky, E.I. Serfeyeva, V.A. Medvedev, J.D. Navratil, Part 12. The Actinide Aqueous Inorganic Complexes, IAEA: Vienna, 1992.
[34] C. Moulin, P. Decambox, P. Mauchien, V. Moulin, M. Theyssier, Radiochim. Acta 52–53 (1991) 119.
[35] K.J. Cantrell, R.H. Byrne, Geochim. Cosmochim. Acta 51 (1987) 597–605.
[36] J.H. Lee, R.H. Byrne, Geochim. Cosmochim. Acta 57 (1993) 295–302.
[37] X.W. Liu, R.H. Byrne, J. Soln. Chem. 27 (1998) 803–815.
[38] K.J. Cantrell, R.H. Byrne, J. Soln. Chem. 16 (1987) 555–566.
[39] D.C. Koningsberger, R. Prins, X-Ray Absorption: Principles, Applications, Techniques of EXAFS, SEXAFS, and XANES, John Wiley & Sons, New York, 1988.
[40] J.J. Rehr, J. Mustre de Leon, S. Zabinsky, R.C. Albers, Phys. Rev. B 44 (1991) 4146.
[41] A.E. Martell, R.M. Smith, R.J. Motekaitis, Critically Selected Stability Constants of Metal Complexes Database, 3.0 ed., Texas A&M University: College Station, TX, 1997.
[42] A. Mochizuki, K. Nagashima, H. Wakita, Bull. Chem. Soc. Japan 47 (1966) 755.
[43] S. Voliotis, A. Rimsky, J. Faucherre, Acta Crystallogr., Sect. B 31 (1975) 2607–2611.
[44] S. Voliotis, A. Rimsky, Acta Crystallogr., Sect. B 31 (1975) 2620–2622.
[45] D.E. Henrie, R.L. Fellows, G.R. Choppin, Coord. Chem. Rev. 18 (1976) 199–224.
[46] R.L. Cone, R. Faulhaber, J. Chem. Phys. 55 (1971) 5198.
[47] H. Wimmer, J.I. Kim, R. Klenze, Radiochim. Acta 58–59 (1992) 165–171.
[48] P. Barthelemy, G.R. Choppin, Inorg. Chem. 28 (1989) 3354–3357.
[49] T. Kimura, Y. Kato, J. Alloys Comp. 271 (1998) 867–871.
[50] J.V. Beitz, J. Alloys Comp. 207–208 (1994) 41–50.